Model-free simulations for compressible mixing layer

Afroz Javed, Debasis Chakraborty and P J Paul

Proceedings of the Institution of Mechanical Engineers, Part G: Journal of Aerospace Engineering published online 1 June 2012
DOI: 10.1177/0954410012446570

Original Article

Institution of MECHANICAL ENGINEERS
Journal of AEROSPACE ENGINEERING

Proc IMechE Part G:
J Aerospace Engineering
0(0) 1–15

DOI: 10.1177/0954410012446570
uk.sagepub.com/jaero
SAGE

Model-free simulations for compressible mixing layer

Afroz Javed[1], Debasis Chakraborty[1] and PJ Paul[2]

Abstract

Confined supersonic mixing layer is explored through model-free simulations. Both two- and three-dimensional spatio-temporal simulations were carried out employing higher order finite difference scheme as well as finite volume scheme based on open source software (OpenFOAM) to understand the effect of three-dimensionality on the development of mixing layer. It is observed that although the instantaneous structures exhibit three-dimensional features, the average pressure and velocities are predominantly two-dimensional. The computed wall pressures match well with experimental results fairly well, although three-dimensional simulation underpredicts the wall pressure in the downstream direction. The self-similarity of the velocity profiles is obtained within the duct length for all the simulations. Although the mixing layer thicknesses differ among different simulations, their growth rate is nearly the same. Significant differences are observed for species and temperature distribution between two- and three-dimensional calculations, and two-dimensional calculations do not match the experimental observation of smooth variations in species mass fraction profiles as reported in literature. Reynolds stress distribution for three-dimensional calculations show profiles with less peak values compared to two-dimensional calculations; while normal stress anisotropy is higher for three-dimensional case.

Keywords

Compressible mixing layer, model-free simulation, three-dimensionality

Date received: 17 October 2011; accepted: 3 April 2012

Introduction

Computational fluid dynamics (CFD) simulations are now routinely used in the scramjet engine development cycle to determine optimal fuel injector arrangements, investigate trends noted during testing, and extract various measures of engine efficiency. One of the most important aspects of the engine efficiency is mixing of fuel and oxidiser streams. In scramjet engines, this mixing takes place along the length of the combustor at very high speeds and compressible conditions, in a confined environment. The understanding of compressible mixing layer becomes necessary to address the issues related with mixing and combustion in a scramjet engine.

It has been observed through various experimental studies that the compressibility effects tend to decrease the growth rate of a high-speed mixing layer as compared to its incompressible counterpart at the same velocity ratio and density ratio.[1–6] Most of these studies have been carried out on free mixing layers which do not have any wall interaction. In practical scramjet combustors with rectangular cross sections, the fuel air mixing streams are confined in the top and bottom direction as well as in the sides. The effects of these walls have been studied using stability analysis and numerical simulations. For a shear layer inside a rectangular channel, Tam and Hu[7] showed that the coupling between the motion of the shear layer and the acoustic modes of the channel produces new instability waves for the spatially growing mixing layers. It was shown by Greenough et al.[8] that there were two general types of instabilities: confined Kelvin–Helmholtz mode and supersonic wall modes, by analysing the effect of wall on a confined compressible temporal mixing layer. Zhuang et al.[9] carried out instability analysis for confined mixing layer

[1]Defence Research and Development Laboratory, India
[2]Department of Aerospace Engineering, Indian Institute of Science, India

Corresponding author:
Debasis Chakraborty, Defence Research and Development Laboratory, Kanchanbagh PO, Hyderabad 500058, India.
Email: debasis_cfd@drdl.drdo.in

and it was argued that the increased instability of the confined mixing layer was due to the feedback mechanism between the growing supersonic shear layer and the wave system (wall reflections) that makes the shear layer more unstable, than the corresponding free supersonic shear layer, which loses energy to acoustic radiation to the far field. Morris et al.[10] further showed that the choice of width-to-height ratio of the confining duct may determine whether the two- or three-dimensional (2D/3D) mode has a greater growth rate. For certain aspect ratios cross sections, it has been observed that the 2D simulations are sufficient to represent the flow field. A number of 2D numerical studies[11–14] have shown a good match with the experimentally observed growth rate, velocity, and pressure data, indicating that the flow field for the mixing layer experiments carried out in a confined environment may be 2D in nature.

Fiedler et al.[15] have described three conditions or mechanisms for the evolution of three-dimensionalities, which are (a) three-dimensionality of the basic flow, (b) three-dimensionality by geometry, and (c) secondary three-dimensionality by flow structure development. In their study of confined mixing layers, Lu and Wu[11] have argued that the presence of lateral confining walls suppress the spatial growth rate of the 3D disturbances. In the absence of the first two mechanisms described by Fiedler et al.[15] and the suppression of secondary three-dimensionality by structural development due to the lateral walls, the flow field in most of the experimental studies with side walls is essentially 2D. The two-dimensionality of the flow further depends on the width-to-height ratio of the confining duct as shown by Morris et al.[10] Two-dimensional simulations were carried out by Lu and Wu[11] for convective Mach numbers ranging from 1.05 to 1.77. The growth rates observed numerically was compared with experimental results and found in good match, confirming the 2D nature of the experimental flow-field. Liou et al.[12] have also shown a good match for the vorticity growth rates of supersonic mixing layers with convective Mach number when compared with experimental results, by performing 2D direct numerical simulation using Euler's equations for convective Mach numbers ranging from 0.14 to 1.28. A reasonably good comparison of wall pressures have been shown for a 2D viscous confined simulation of supersonic mixing layer, at a Convective Mach number around 0.79, by Chakraborty et al.[13] using model-free simulation. Li and Fu[14] solved 2D Boltzman equations for high-speed planar free mixing layers with convective Mach numbers ranging from 0.2 to 1.0. They found out that the mean velocity field and the thickness growth rate for the 2D mixing layers agree generally well with the experimental results even though the 'real' flow is 3D. However, the 2D simulations significantly over predict the velocity fluctuation intensities and shear stresses compared with experimental data, especially in cases with high convective Mach numbers. All these 2D studies compared their results with the experiments having confining side walls, which may have made the flow field 2D.

Two-dimensional inviscid eddy simulations were carried out for free supersonic mixing layers with convective Mach numbers ranging from 0.35 to 0.7 by Oh and Loth[16] using finite element method (FEM) techniques. The computed growth rate at convective Mach number 0.45 showed significantly under predicted values when compared to a 3D direct numerical simulation (DNS) results after a certain axial location. This under prediction is attributed to the presence of both oblique and streamwise vorticity which contributes to additional instability modes and allows for vortex stretching, which could have been suppressed with the presence of side walls.

It is clear from the above discussion that the role of oblique disturbances in the growth and the development of supersonic confined mixing layer need further investigation. It was argued[9,11] that the coupling between the motion of the shear layer and the duct acoustics waves produce a new instability mechanism namely the 'supersonic instability' which is predominantly 2D in nature. This instability mechanism originates from wall confinement and is different from the classical Kelvin–Helmholtz instability. However, adequate studies are not reported in the literature addressing the role of three-dimensionality on the growth and development of confined supersonic mixing layer in high convective Mach number range.

In the present study, different 2D and 3D model-free simulations were carried out to understand 3D effects in the growth and development of confined supersonic mixing layer. Mixing of two high-velocity streams of hydrogen and nitrogen at static temperatures of 103 and 2436 K, respectively, investigated by Erdos et al.[17] has been taken as a test case. The adequate length of test section for flow development, cleanliness of the geometry, detailed flow visualisation, measurement of surface parameters are some of the notable features for selecting the experiment for validation case. In the experimental setup, the mixing of two high-speed streams takes place in a duct of rectangular cross section without any divergence. Another important feature of this experimental condition is the high difference in the molecular weight and temperature of the two mixing streams, which is not there for other available experimental studies data. Instantaneous and averaged properties of various flow variables and turbulent quantities obtained from 2D and 3D simulations were compared to bring out the effect of three-dimensionality in the confined supersonic mixing layer development.

Numerical simulation of the mixing layer

The parameters for the mixing layer simulations in the present work are taken from an experimental study carried out by Erdos et al.[17] In one of the experimental cases of their study, hydrogen and nitrogen at Mach numbers of 3.09 and 3.99, respectively, flow in the upper and lower parts of a rectangular duct, forming a mixing layer. A schematic of the Experiment along with the flow parameters is shown in Figure 1. The cross section after the splitter plate is 25.4 mm high and 50.8 mm wide.

The primary stream is fed through an expansion tube, while the secondary stream is supplied through the single manifold of two Ludweig tubes. The wall heat transfer rates from the experimental data indicate a laminar entry at the splitter plate, transition zone just after that, and fully turbulent flow after a downstream distance of roughly 300 mm from the splitter plate.

For the experimental condition chosen for numerical simulation, nitrogen stream makes primary flow at the lower part of the duct coming from an expansion tube, while the upper part of the duct makes secondary flow of hydrogen coming from Ludweig tubes. The details of the flow parameters are presented in Table 1. The convective Mach number is 0.79 for this experimental condition.

Computational methods

In the present study, model-free simulation is used. A model-free simulation is numerical simulation without any turbulence model. The Navier–Stokes equations with continuity, energy transport and species transport equations are solved without any time averaging. Unlike DNS, in a model-free simulation, the resolution of Kolmogorov scales is not sought for. However, the grid size in case of model-free simulation is such as to resolve the large-scale fluctuations affecting the formation and growth of mixing layer. Very small-scale fluctuations responsible for the transfer of turbulent mechanical energy to the thermal energy may not be fully resolved.

Compact finite difference scheme – method, grid and boundary conditions. Two-dimensional model-free simulations are carried out by employing nonreacting version of SPARK2D code developed at the NASA LaRC by Drummond and Carpenter.[18] It discretises 2D Navier–Stokes equations by using Mac-Cormack's compact scheme with fourth-order spatial and second-order temporal accuracy. This choice represents a compromise between the accuracy of higher order numerical algorithm and the robustness and efficiency of low-order methods. This code has been validated by comparing the computed results of some test problems with known analytical solutions. Carpenter and Kamath[19,20] have demonstrated that with the compact scheme, the growth rate with the initial profile based on the eigenfunctions predict those from linear stability theory for free shear layer to within 1% for a time duration equal to about 5 times the sweep time of the flow field. The compact scheme provide a substantial reduction in truncation and phase errors over the first-order upwind and the second-order Mac-Cormack's scheme.

The flow domain is of size 535 mm × 25.4 mm. The two streams are separated by a splitter plate at a height of 12.7 mm, before the start of mixing. The grid is stretched exponentially in the axial direction with

Table 1. Inflow parameters for confined supersonic mixing layer.

Location	Primary	Secondary
Species	Nitrogen	Hydrogen
Velocity (m/s)	3807	2389
Temperature (K)	2436	103
Pressure (MPa)	0.02758	0.02758
Mach number	3.78	3.09
Re (/mm)	2200	42,000

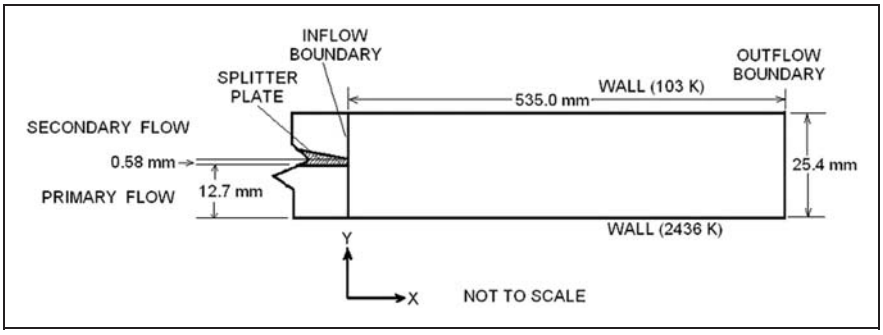

Figure 1. Schematic of experimental condition of Erdos et al.[17] for confined supersonic mixing layer.

minimum grid spacing at the inflow boundary to capture the initial development of the mixing layer. In the lateral direction, minimum grid spacing is taken near the interface and it is stretched exponentially towards both the upper and lower wall. The wall boundary layer is resolved by taking very fine mesh near the solid wall and the grid is again stretched exponentially in the region away from the wall. The grid structure employed in the simulations has 1000 points in the axial direction with minimum grid size of 0.3 mm near the inflow boundary plane and the maximum size of 0.8 mm near the outflow boundary. In the lateral direction, 101 grid points are used with a minimum grid spacing of 0.09 mm near the interface and wall, and the maximum grid spacing is of the order of 0.5 mm in the region away from interface and wall. The grid considered in the simulation is sufficient to capture the large-scale structure of the flow field as is evident from the grid resolution studies. Grid resolution calculations were made by varying the number of grids in both axial and lateral directions. In this grid resolution study, five different grids namely, 1000×101, 750×101, 500×101, 500×125, and 500×75 were used to determine the effect of grid resolution in the axial and cross-stream directions. One sweep time for the flow is assumed as the time taken for the flow to cross the domain with lower velocity stream. The results for first two such sweep times are discarded, and the variables are averaged for next two sweeps. The value of averaged axial velocity at a plane 300 mm from the inlet is shown in Figure 2(a) and (b) for both lateral and axial refinement of the grids. It can be observed that increasing the number of grids from 500 to 1000 in axial direction and 75 to 125 in the lateral direction leaves the results almost unchanged. The spectral content of pressure fluctuations were compared with different grid and is observed that not only the mean values, but also the amplitudes of the fluctuations match well with different grid. Hence, it is concluded that the 1000×101 grid is sufficient to give grid-independent solution.

The boundary conditions set for this problem are as follows. In the solid boundary at the upper and lower walls, no slip conditions for the velocities and the constancy of wall temperatures are imposed. A boundary layer velocity profile is given at the inlet as shown in Figure 3. The thicknesses of boundary layer were taken from the experimental data in both the streams at the inlet. In the boundary layer regions, parabolic profiles are given to match the free stream velocity. The effect of fluctuations with time in the inlet velocity profiles are studied by comparing the root mean square (rms) values of velocity fluctuations at different axial locations with and without initial forcing. The lateral distribution of velocity fluctuations (rms values) at different axial locations ($x = 100$, 200, 300, 400, and 500 mm) are compared in Figure 4. It can be observed that the initial forcing does not have any influence in

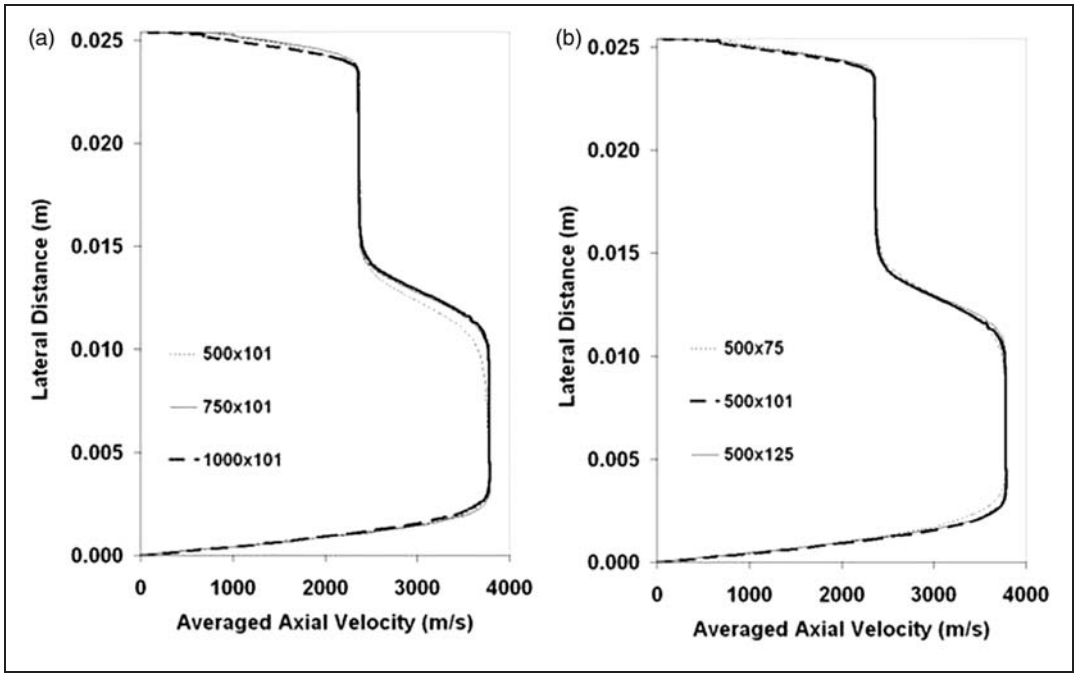

Figure 2. Averaged axial velocity variation in lateral direction at an axial location of 300 mm obtained with grid refinement in (a) lateral direction (b) axial direction.

the development of flow features in the downstream region. Both the streams are given equal pressure of 27,580 Pa. Nitrogen mass fraction is set to unity for primary stream, while hydrogen mass fraction is unity for the secondary stream. The static temperatures of both primary and secondary streams are set at constant values of 2436 and 103 K, respectively. The exit boundary condition is obtained by second-order extrapolation and is considered satisfactory for this problem dominated by supersonic flow.

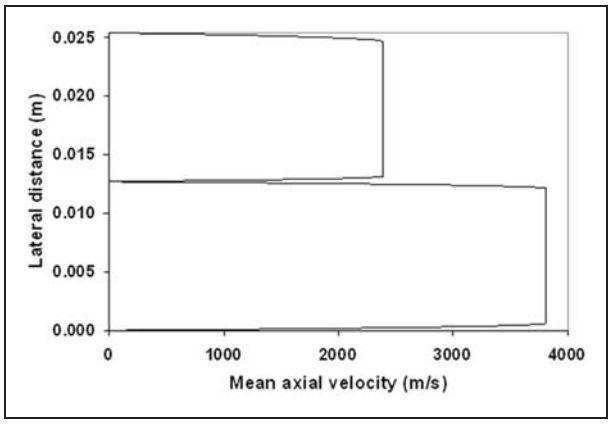

Figure 3. Axial mean velocity profile at the inlet (edge of splitter plate).

The mean properties of the flow can be calculated after the initial conditions have been purged out of the flow domain. The fluid speed inside the domain varies from zero at the walls to the speed of the high-speed stream. In this situation, it is difficult to assign a characteristic speed which could be indicative of purging time. In order to evaluate the time needed to purge out the initial conditions, a third chemical species is added in the initial condition, and its concentration is monitored. Similar method has been adopted to check the purging of initial conditions by Lian et al.[21] for their unsteady simulation of a combustor. The initial condition for the species is given as mass fraction of 0.5 of an inert species in the entire flow domain to serve as a 'marker' for ascertaining the purging of initial conditions. The monitoring of this inert species shows that it takes 515 μs for its maximum mass fraction to become less than 1×10^{-6} within the entire flow domain. Changing the initial conditions with different velocities also does not change this purge time. The averaging process for the evaluation of mean quantities is started after this purging time of 515 μs.

The attainment of statistical steady state is checked by averaging the values of the required variables over time, after the purging of initial conditions. Different flow variables are averaged as the solution proceeds; and these values are checked at different intervals for stabilised values. The time interval chosen for checking

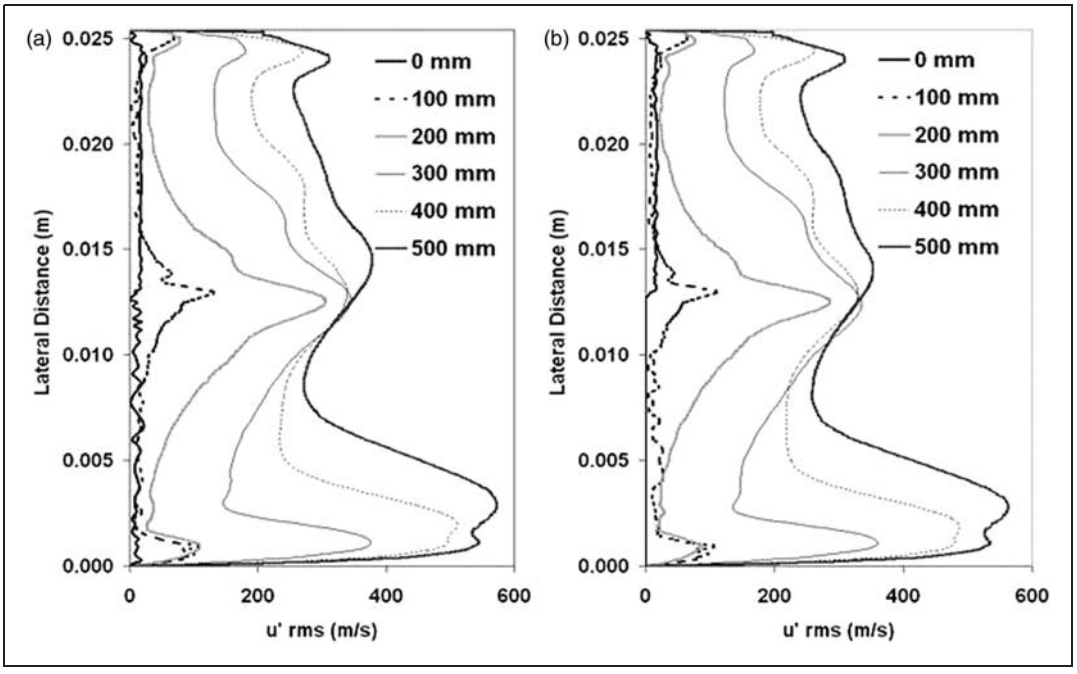

Figure 4. Root mean square values of fluctuations in average axial velocity at different axial locations (a) both primary and secondary streams are forced (b) only secondary stream forced.

the stabilisation of averaged quantities is taken same as that taken for purging the initial condition, that is, 515μs. This time interval is referred as one sweep time for the purpose of checking the attainment of statistical steady state. It has been observed that the mean properties like velocities, temperature, and species mass fractions stabilise at less number of sweeps than the turbulence statistics quantities like Reynolds stress and Reynolds fluxes, etc. It was found that all the mean and turbulent quantities reach their statistical steady state after four sweeps of run. The variation of averaged axial velocity and Reynolds stress in lateral direction at an axial location of 500 mm, with number of sweeps are shown in Figure 5. The final average values of the variables are taken by averaging the instantaneous values for time taken for four sweeps that is 2060 μs.

2D and 3D OpenFOAM simulations – method, grid and boundary conditions. OpenFOAM open source software (www.openfoam.com) is used to carry out model-free studies for a 3D domain as well as a 2D domain. OpenFOAM is free-to-use open source numerical simulation software with extensive CFD and multi-physics capabilities. The governing equations are discretised using polyhedral finite volume method. The second-order accuracy in space and second-order accuracy in time is used. The object-orientation of the software facilitates easy model implementation in physical modeling and numerics (discretization, solvers, equation coupling). In the present case, mass conservation equation, momentum conservation equation, energy conservation equation in the static enthalpy form, and species conservation equation are solved. The thermochemical properties of the species involved are read from JANAAF tables. The Lewis number and Schmidt number are set to unity.

The grid and boundary conditions used for 2D OpenFOAM simulations are same as those used for SPARK simulations. For 3D calculation, a 3D computation mesh with 41 planes is formed by spanning the 2D grids with an equal distance in the z-direction. The distance between two planes is kept to be 0.5 mm. The boundary condition at the side walls is set as periodic boundary condition. In order to have a sufficiently developed flow field before the mixing of the streams, the inlets with splitter plate are extended upstream by a distance of 50 mm. A splitter plate with a constant thickness of 0.58 mm is provided in this stretched length. The velocities at the splitter plate walls are kept zero, and adiabatic wall conditions are employed for heat transfer. In case of Open FOAM simulations also, a parabolic boundary layer profile is given near the walls and the splitter plate. The purging time for initial conditions is taken same as evaluated from the SPARK simulations. The time taken to reach

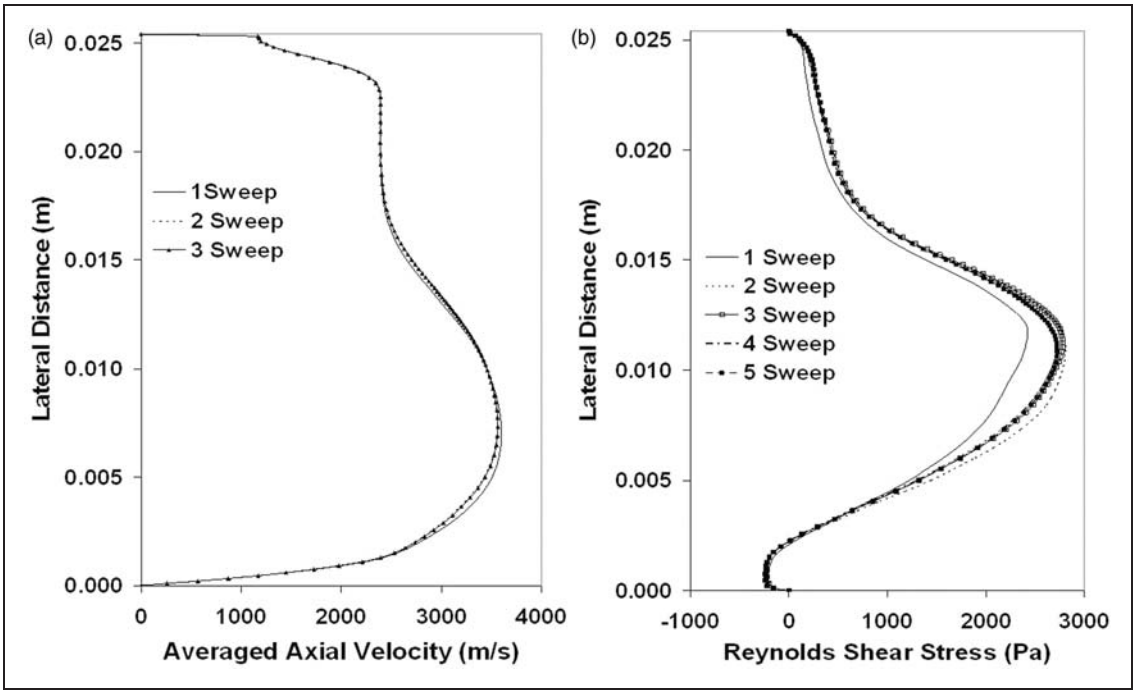

Figure 5. Variation of the averaged variables with sweep times in the lateral direction at an axial location of 500 mm: (a) axial velocity, (b) Reynolds shear stress.

statistical steady state is also taken same as evaluated from SPARK simulations.

Results and discussion

The instantaneous values and averaged values of Hydrogen mass fraction and axial velocity, from 3D OpenFOAM simulations, are shown in Figures 6 and 7, respectively, at different axial locations. In these figures, the *y*-axis shows lateral direction while the *z*-axis represents span wise direction. The three-dimensionality of the instantaneous flow field can be clearly observed in both the species and axial velocity distributions. Similar kind of three-dimensionality is noticed in the experimental results of Clemens and Mungal[22] above a convective Mach number 0.6. Sandham and Reynolds[23] have also shown through linear theory and direct simulation that above convective Mach number 0.6, the mixing layer would have a strongly 3D behaviour. The time average values can be observed to be 2D. This two-dimensionality is also noticed in the experimental results of Wantuck et al.[24] Although the instantaneous flow field is 3D, the averaged flow field of the mixing layer is observed to be 2D.

In the present simulation, no fluctuations in the velocity fields at inlet are introduced. This is in agreement with the almost laminar entry conditions observed in the experiment. This laminar entry condition shows transition to turbulence with the development of turbulent kinetic energy (TKE), as shown in Figure 8. It can be observed that the mixing layer shows very small TKE in the beginning and with the development of

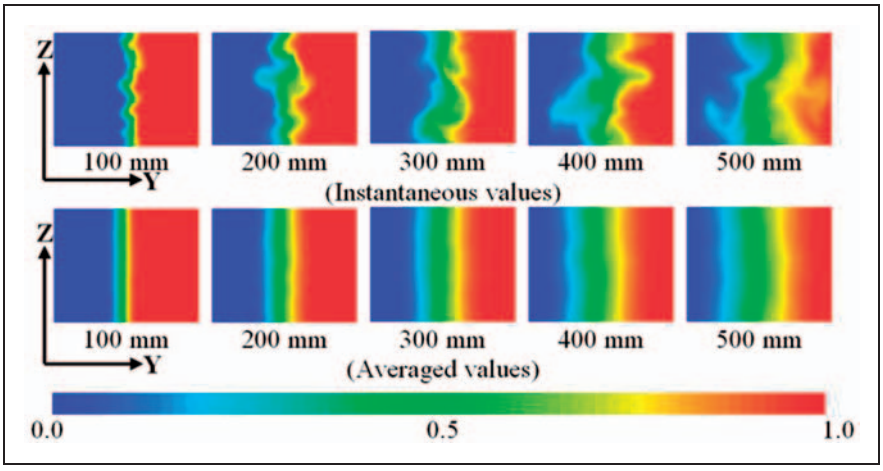

Figure 6. Instantaneous and averaged distribution of H_2 mass fraction at different axial locations.

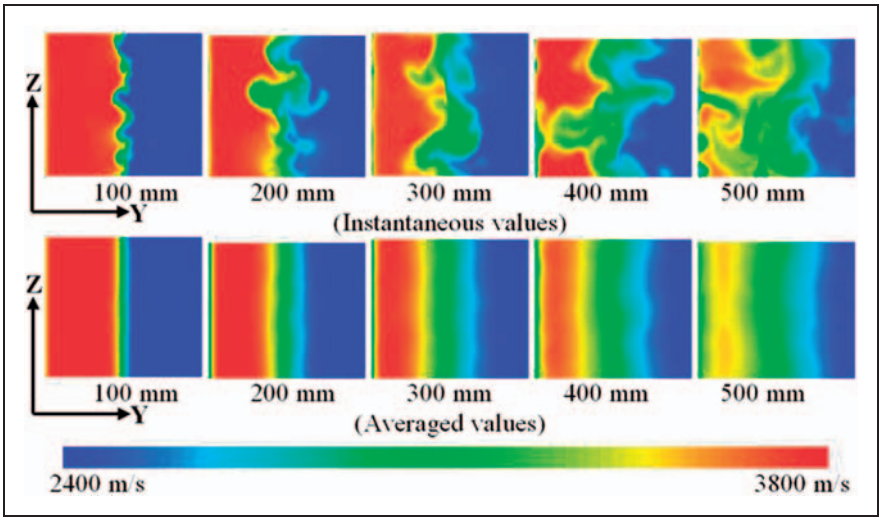

Figure 7. Instantaneous and averaged distribution of axial velocity at different axial locations.

the flow, the TKE increases indicating onset of turbulence. Instantaneous vorticity contour in the test section is shown in Figure 9 which clearly depicts the development of large-scale structure in the mixing layer, vortex roll up and tearing and pairing of vortices.

The mixing layer thickness is obtained using the 10% ΔU thickness definition in the growth region, where ΔU is calculated as the difference between local free stream velocities of the mixing streams. The thickness comes as the distance between two points where the velocities are $(0.1U_1 + 0.9U_2)$ and $(0.9U_1 + 0.1U_1)$. Mixing layer thicknesses are evaluated at different axial locations for the simulation results using 2D SPARK code, 2D OpenFOAM, and 3D OpenFOAM. The mean axial velocity is normalised as $\bar{U} = (U - U_1)/(U_2 - U_1)$ and plotted against a similarity lateral co-ordinate $\eta = (y - y_0)/b$, where y_0 is the location in lateral direction with the mean axial velocity as $(U_1 + U_2)/2$ and b is shear layer thickness. The similarity profiles at different axial locations are shown in Figure 10(a) to (c) for all the simulations. It can be observed from Figure 10(a) that it takes around 300 mm axial distance for the self-similarity to be established in case of SPARK simulations. While in case of both 2D and 3D simulations from OpenFOAM self-similarity is achieved after 200 mm of the axial distance as can be seen in Figure 10(b) and (c). It can be observed that the flow field for all the simulations achieves self-similarity within the duct length.

The mixing layer thicknesses in the self-similar region are plotted in Figure 11 for different simulations. Also an empirical growth rate is evaluated using Langley curve for the present velocity ratio, density ratio, and convective Mach number and shown in the same figure. Although the thicknesses of the mixing layer predicted using different simulations are different, the slopes of these curves shown in Figure 11 do not seem to differ much. The growth rates observed from the 2D OpenFOAM and 2D SPARK are found to be 30.8 and 33.8 mm/m, respectively. While the growth rates predicted 3D OpenFOAM simulations is found to be 37.7 mm/m. Three-dimensional natures of the disturbances are responsible for this enhanced growth rate for 3D simulation. The growth rate for similar free shear layer from Langley curve comes out to be around 23.0 mm/m. The 2D simulation results from OpenFOAM and SPARK are near to each other with a difference of <10%; however, these results show growth rate higher by around 30% when compared with Langley free shear layer growth rate. The 3D simulation results show around 40% more growth rate than the free shear layer growth rate. This increased growth rate may be due to the effect of confinement, difference in temperature ratio, molecular weight ratios, inlet conditions, etc., which are not considered for the evaluation of growth rates from Langley curve, while the present case deals with a confined mixing layer of two streams with different molecular weight and temperatures. However, the increased growth rate as well as the higher thicknesses in the results from 3D OpenFOAM simulations, when compared with 2D simulations is due to the 3D nature of the flow-field. It is observed that the three-dimensionality destabilises and destroys 2D structures responsible for mixing suppression, resulting in increased mixing.[15] In a series of DNS simulations carried out for a free supersonic mixing layer with convective Mach numbers ranging from 0.2 to 1.56 by Risha[25] for both 2D and 3D supersonic free shear layers, it was observed that the shear layer growth rate was significantly higher for 3D cases than the 2D cases with the ratio of 3D to 2D growth rates varying between 1 and 4.7, indicating more mixing for a 3D situation. Oh and Loth[26] have considered some computational studies for

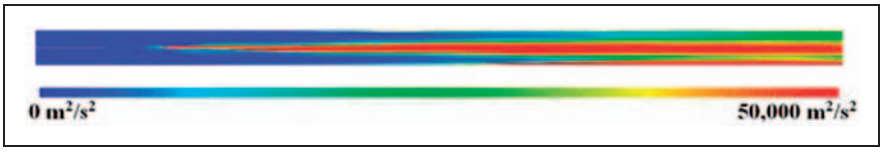

Figure 8. Turbulent kinetic energy (TKE) distribution along the length of the duct.

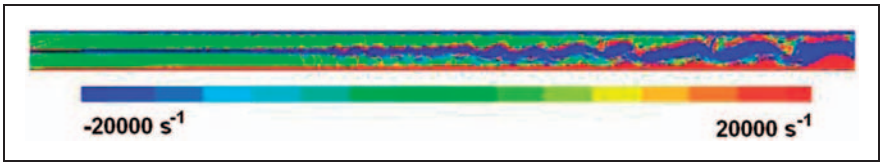

Figure 9. Instantaneous vorticity distribution in the test section.

2D and 3D simulations, and shown that the mixing layer thickness matches well near the splitter plate with empirical growth rate, but as the distance increases the thickness is under predicted while in the case of 3D simulations the increased growth rate is captured.

The bottom (Nitrogen side) and top (Hydrogen side) wall surface pressures obtained from different model-free simulations (2D SPARK and 3D OpenFOAM) are plotted in Figures 12 and 13, respectively. The experimental pressure data from Erdos et al.[17] are also plotted in the same figures.

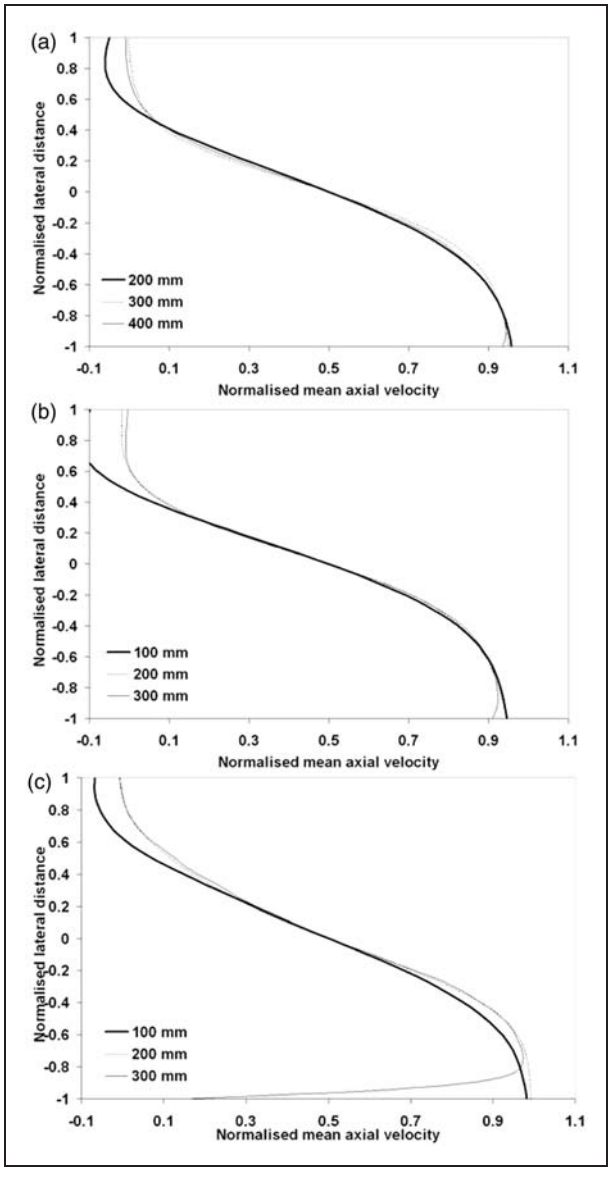

Figure 10. Self-similarity profiles at different axial locations for: (a) SPARK simulations, (b) OpenFOAM 2D simulations, and (c) OpenFOAM 3D simulations.

The 2D simulations performed using OpenFOAM and SPARK show a satisfactory comparison in wall pressures. In the downstream direction for the Hydrogen side wall, the predictions from the 2D OpenFOAM simulation are on a lower side. Considering the repeatability and error band of the experimental data, as reported in Erdos et al.,[17] the comparison can be considered reasonable.

The 3D simulation is carried out taking a span of 20 mm in the z-direction ranging from –10 mm to 10 mm. The pressure values are taken at planes passing through −9, −5, 0, 5 and 9 mm. These pressures are also plotted in Figures 12 and 13. The wall pressure values predicted by 3D simulation using OpenFOAM shows a good match for first 200 mm of the flow with the experimental results. For some initial distance, the 2D and 3D simulation from OpenFOAM show very good match. Afterwards the 3D simulation results show lower values for the wall pressure. These low values of the pressures can be attributed to the scheme of the discretisation as well as the distribution of momentum in the third direction. Nevertheless, the collapse of the pressure data for all the five planes indicates that the averaged flow is essentially 2D in nature.

The lack of match for the far downstream point from experimental data and 3D open FOAM results can be attributed to the absence of side walls in the simulations. According to Lu and Wu[11] the side walls act as suppressors for three-dimensionality and the flow essentially remains 2D. This suppression of three-dimensionality by side walls could explain the better match of experimental pressures data with 2D simulations data.

The pressure in a fluid flow is defined as the normal stress on a fluid element. While averaging of the flow data from simulation results, the normal components of Reynolds stress also add to the normal stress. In the case of wall pressure, the simple time averaging of pressure variable alone from model-free simulation data gives correct picture of pressure, as the normal components of Reynolds stress are zero at wall. But in the case of pressure values in transverse direction, the value of averaged transverse Reynolds stress needs to be added to the average pressure value. This has been done for the simulation data and it is plotted at axial locations of 200 and 300 mm, as shown in Figure 14(a) and (b). Two-dimensional OpenFOAM data shows a comparable pressure values with those predicted using 2D SPARK code. It appears that the use of lower order spatial accuracy does not affect the prediction of pressures much. The pressure distribution obtained from the 3D simulations shows a lower value than the pressures predicted by all the other methods. However, the shape of the pressure distribution curve by 3D OpenFOAM closely follows the 2D OpenFOAM

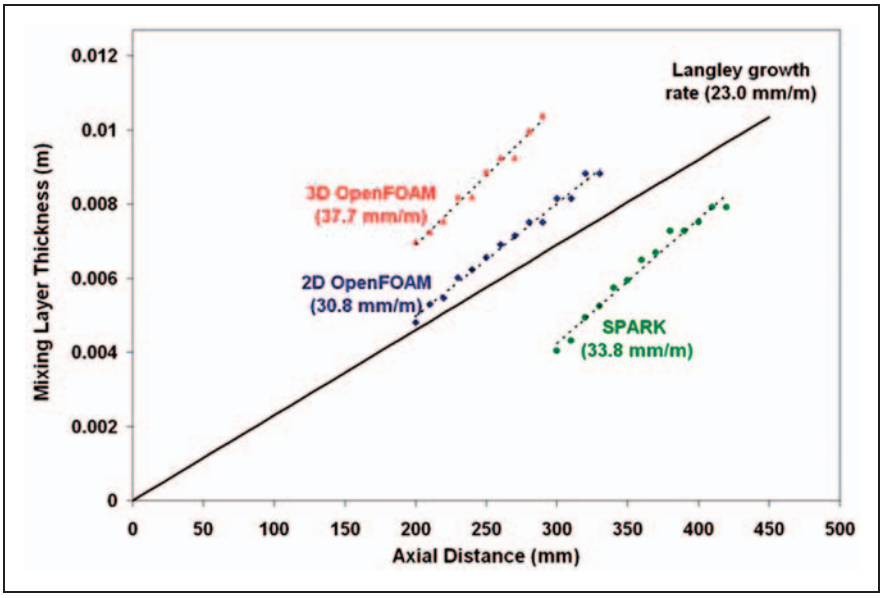

Figure 11. Mixing layer thicknesses and corresponding growth rates from different simulations.

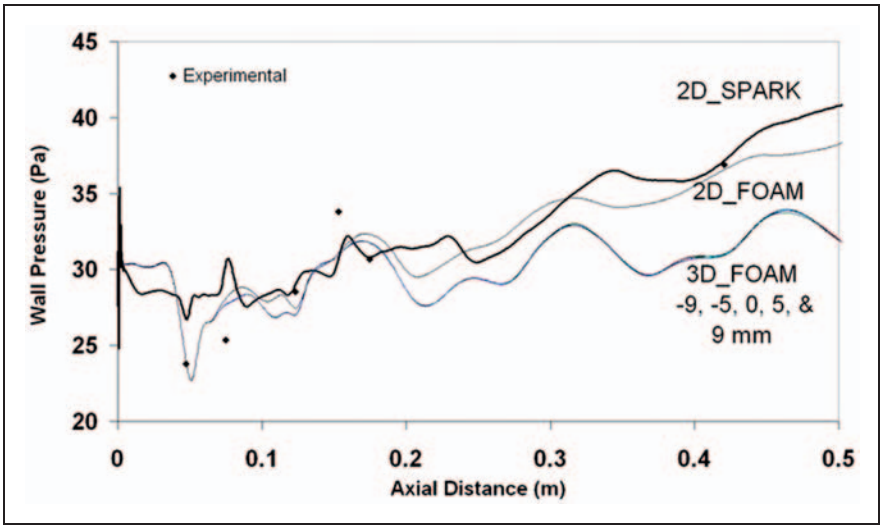

Figure 12. Bottom wall (Nitrogen side) pressure comparison among experimental and numerical results.

simulation results with lower values, indicating the effect of relief in third direction.

The axial mean velocity distributions at different cross sections are shown in Figure 15(a) and (b). The 3D OpenFOAM simulation results show a higher mixing layer thickness at all the axial locations when compared with 2D OpenFOAM results as a consequence of three-dimensionality. Similar results are reported by Risha[25] for the free shear layer simulations. 2D SPARK results show a lower mixing layer thickness than 2D OpenFOAM results, due to late establishment of flow and achievement of self-similarity. However, after the achievement of self-similarity, the SPARK results show a slightly higher growth rate than that predicted by 2D OpenFOAM. The earlier establishment of flow, in case of OpenFOAM occurs due to presence of the upstream region in the inlet zone.

The distribution of static temperature at axial locations of 300 and 500 mm is shown in Figure 16. Temperature distribution from 2D SPARK simulation and 2D OpenFOAM simulations do not show quite good match except in locations near walls. The thermal mixing is much more in the mixing layer for 2D OpenFOAM simulation results than in case of the 2D SPARK simulation results.

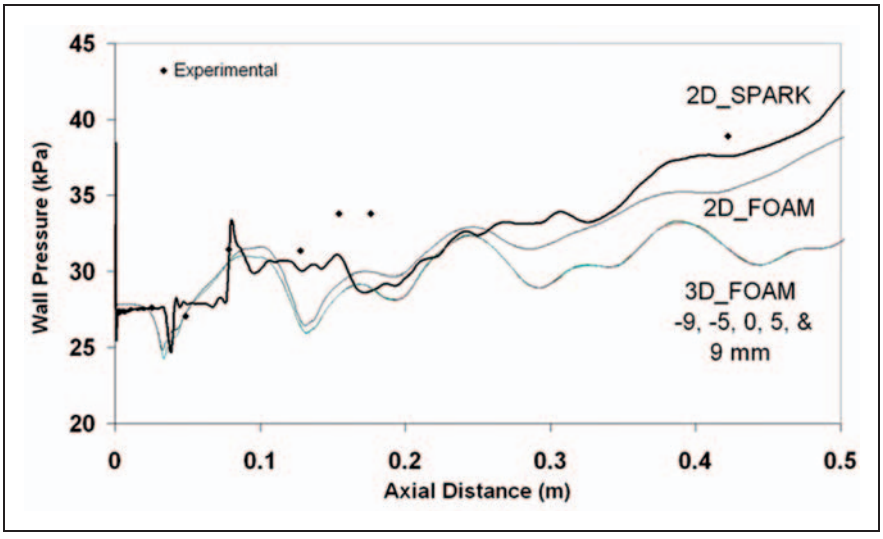

Figure 13. Top wall (Hydrogen side) pressure comparison among experimental and numerical results.

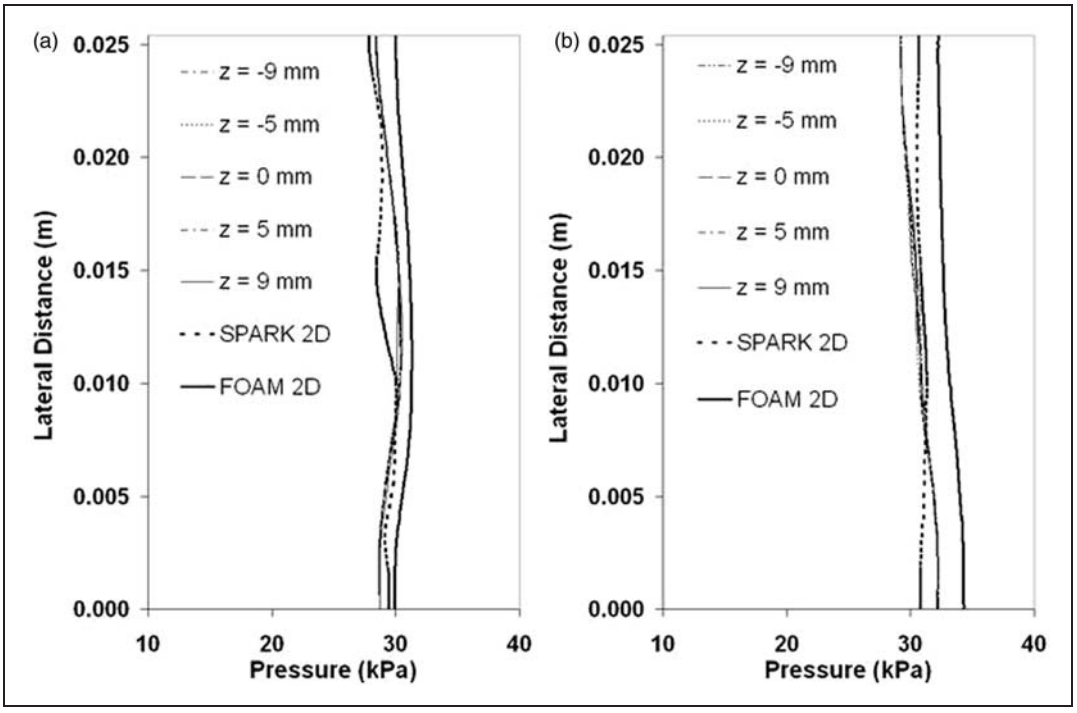

Figure 14. Sum of pressure and lateral component of Reynolds stress at different axial locations: (a) 200 mm, (b) 300 mm.

Comparing 2D and 3D OpenFOAM results for temperature distribution, at 300 mm location, there is no appreciable difference between the two, indicating a very small effect of three-dimensionality on the temperature distribution in the initial stages. At 500 mm location, 2D results show more mixing than the 3D results. Also the peak near higher temperature wall is found larger for 3D than for 2D case. This happens due to more heat transfer to lower temperatures resulting from more mixing in the 2D case. This more mixing in the 2D case happens due to the coupling of species equation, where the increased species mixing in the 2D case causes increased thermal mixing also.

Figure 17 depicts the distribution of hydrogen mass fraction at axial locations of 300 and 500 mm. At 300 mm axial location, the species distribution profiles predicted by all the simulations are smooth and

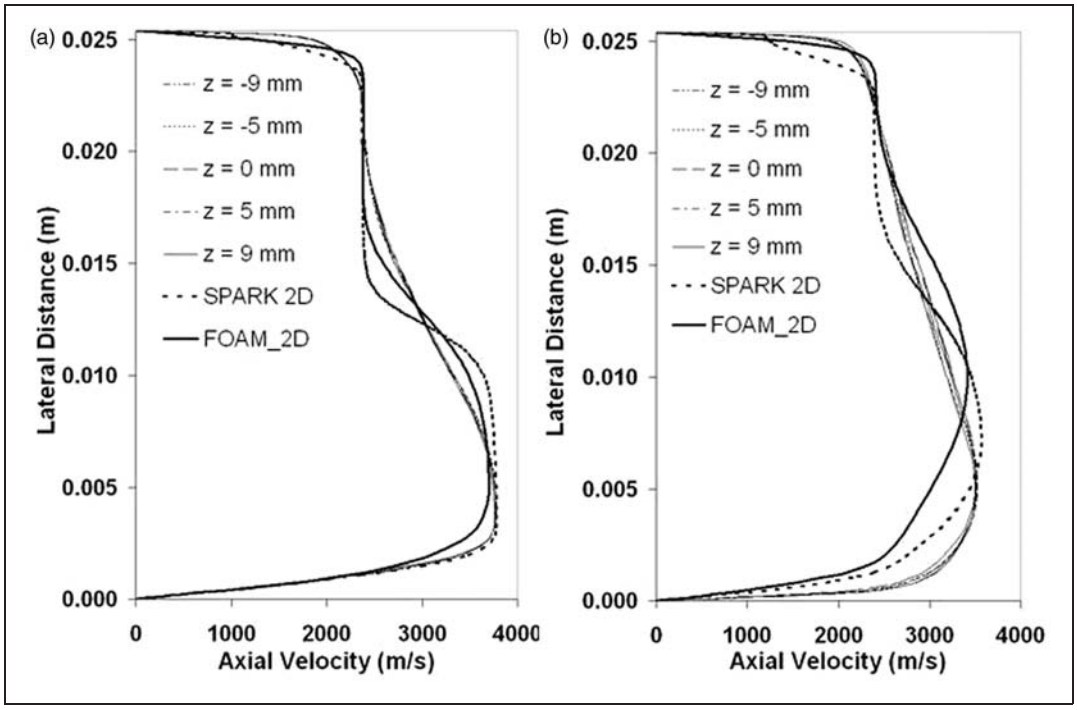

Figure 15. Axial mean velocity distribution at different axial locations: (a) at 300 mm, (b) at 500 mm.

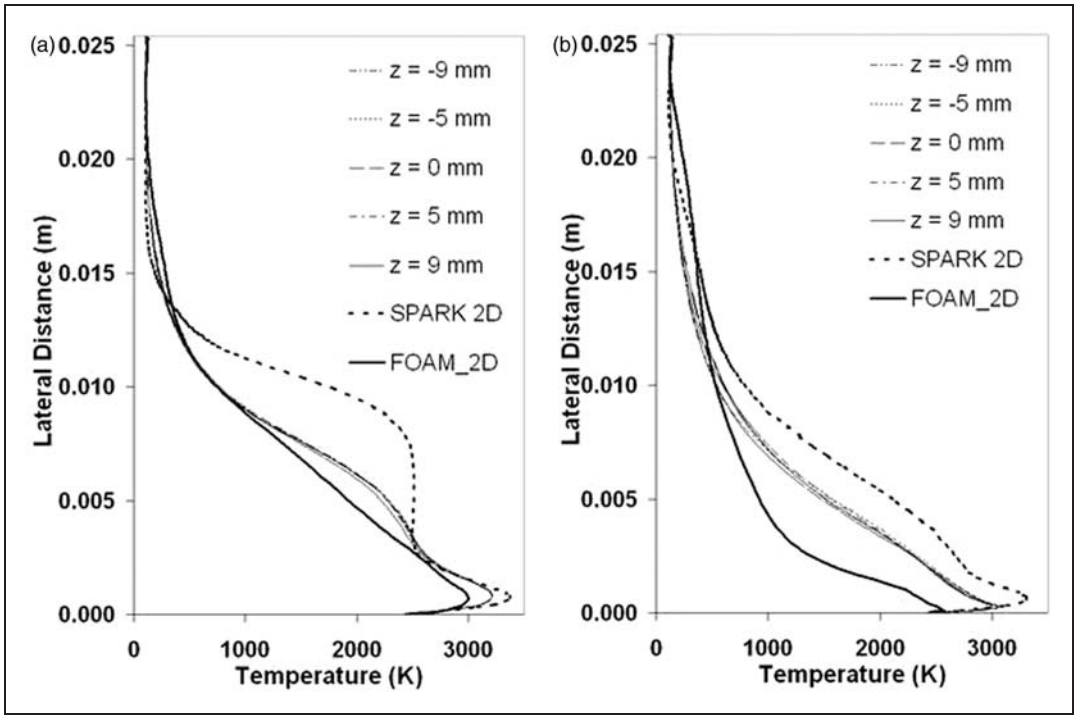

Figure 16. Temperature distribution at different axial locations at: (a) 300 mm, (b) 500 mm.

gradually varying. The same kind of gradual variation is observed in an experimental study carried out by Wantuck et al.,[24] where mixing between supersonic streams of Argon and Helium is studied experimentally at a convective Mach number of 1.2. As the mixing layer progresses downstream, at the axial location of 500 mm, the smooth variation in the species profiles looks to be lost for 2D computations carried out

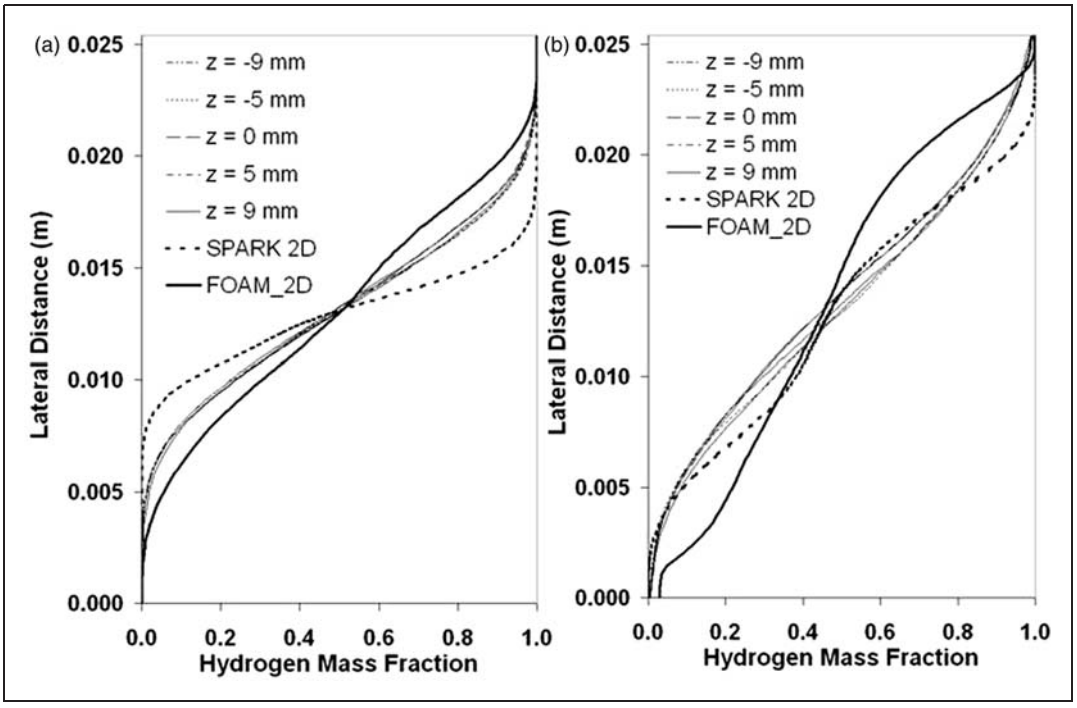

Figure 17. Hydrogen mass fraction distribution at different axial locations: (a) at 300 mm, (b) at 500 mm.

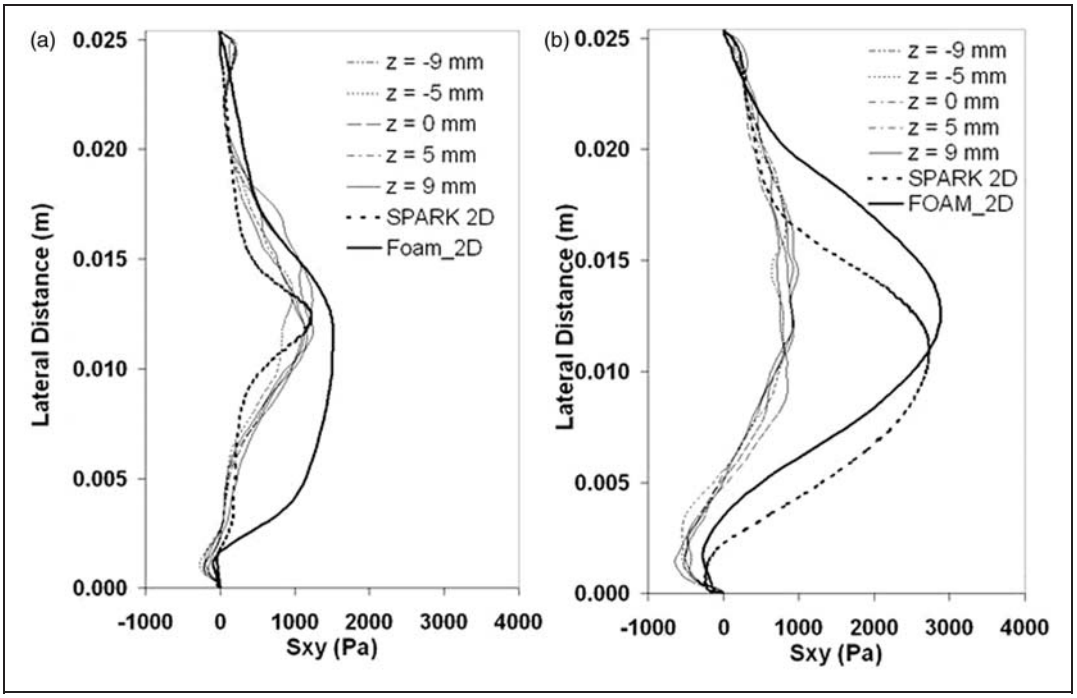

Figure 18. Reynolds shear stress distribution at different axial locations: (a) at 300 mm, (b) at 500 mm.

using both SPARK and OpenFOAM. It appears that although flow variables like velocity and pressure, are predicted satisfactorily with the 2D calculations, in the case of species the predictions are contrary to the experimental findings. These variations of species seem to be affected more with the three-dimensionality of the flow. This higher and non-smooth variation of species affect the temperature profiles also in the mixing

Table 2. Peak values of anisotropy of normal turbulent stresses.

Simulation	$(\sigma_u/\sigma_v)_{max}$	$(\sigma_u/\sigma_w)_{max}$	$(\sigma_v/\sigma_w)_{max}$
2D SPARK	2.50	–	–
2D OpenFOAM	2.01	–	–
3D OpenFOAM	3.43	1.96	0.84

layer as observed in the comparison of static temperatures.

The comparison of the Reynolds shear stress has been shown in Figure 18. The 2D predictions by SPARK code show slightly lower value of peak stress than OpenFOAM in the initial stages of the flow. In the further downstream direction, the 2D SPARK and OpenFOAM results show almost similar distribution of the Reynolds shear stress with slight displacement of the peak value in the lateral direction. The 3D OpenFOAM simulation results show lower peak Reynolds shear stress. Also the three-dimensionality of Reynolds shear stress is evident from these curves, despite a profound two-dimensionality exhibited by the pressure, velocity, temperature, and species mass fraction distribution curves at different locations.

From the two components of Reynolds normal stresses, the anisotropy of the turbulence σ_u/σ_v can be determined for the 2D cases as well as 3D case. The anisotropies σ_u/σ_w and σ_v/σ_w are also evaluated for the 3D case. The peak values of the anisotropy of the different turbulent stresses in the mixing layer region are shown in Table 2.

The reduction in the maximum values of the normal stress anisotropy $(\sigma_u/\sigma_v)_{max}$ for 2D OpenFOAM simulations as compared with 2D SPARK simulations indicates increase in isotropy due to numerical diffusion. This normal stress anisotropy shows a higher value than the 2D OpenFOAM simulations for 3D OpenFOAM simulations, showing increased anisotropy of the flow. Goebel and Dutton[27] reported peak values of this anisotropy to vary from 1.5 to 3.5 for a variation of Convective Mach number from 0.2 to 0.98. A value of 1.32 is reported in literature[28] for normal stress anisotropy $(\sigma_u/\sigma_w)_{max}$ as against the computed value of 1.96. This anisotropy is observed to not vary much with the compressibility. The normal stress anisotropy $(\sigma_v/\sigma_w)_{max}$ is observed to be unity in case of incompressible flows, while the observed value in present computation is 0.84 which is very near to the reported value of 0.85.[27] It can be observed that all the values of anisotropy are away from unity; therefore, it would seem that numerical simulations which are based on isotropic turbulence models may perform poorly at higher convective Mach numbers.

Conclusions

An experimental case[17] of supersonic mixing layer with two parallel supersonic streams of hydrogen and nitrogen is investigated numerically by using model-free simulations. The two streams are at different temperatures and Mach numbers. Numerical studies have been performed using higher order compact scheme SPARK code (fourth-order spatial and second-order temporal) and second-order spatial and temporal finite volume OpenFOAM scheme for both 2D and 3D conditions.

The 3D simulations show the instantaneous flow field to be 3D while the averaged flow field remains essentially 2D as far as pressure and velocities are concerned. Although the thicknesses of the mixing layer predicted using different simulations are different, the slopes of these curves do not seem to differ much. The growth rates observed from the 2D OpenFOAM and SPARK simulations are found to be almost equal and around 30% more than that for a corresponding free shear layer. While the growth rates predicted using and 3D OpenFOAM simulations show around 40% more growth rate than the corresponding free shear layer growth rate. This higher growth rate is expected for 3D mixing layers because of destabilisation and destruction of the 2D structures responsible for mixing suppression.[15] The good match of the pressures with the experimental values from the 2D calculations is indicative of the two-dimensionality of the flow-field inside the test duct for the height-to-width ratio of the duct cross section and convective Mach number considered. It can also be inferred that the presence of side walls can be responsible for reduction in the mixing. The pressure predictions with both 2D simulations seem to match well with slight differences, and the effect of discretisation scheme seems to be minimal. The pressures predicted using 3D OpenFOAM show lower values in the downstream direction, indicating the effect of three-dimensionality.

The temperature and species predictions are quite different for 2D and 3D simulations. The species distribution using 2D simulations does not match the experimental observations of smooth variations. It is interesting to note that while 2D calculations give good match of velocity and pressures with experimental observation they fail to do so in case of species distribution and temperature prediction.

Reynolds stress distributions exhibit significant three-dimensionality with lower peaks compared to 2D calculations. The anisotropy level for 3D calculations is significantly higher. It appears that turbulence models based on isotropic turbulence may not be applicable for predicting the flow field of confined supersonic mixing layers.

References

1. Papamoschou D and Roshko A. The compressible turbulent shear layer: an experimental study. *J Fluid Mech* 1988; 197: 453–477.
2. Elliot GS and Samimy M. Compressiblity effects in free shear layers. *Phys Fluid A2* 1990; 7: 1231–1240.
3. Goebel SG, Dutton JC, Krier H, et al. Mean and turbulent velocity measurements of supersonic mixing layers. *Exp Fluids* 1990; 8: 263–272.
4. Goebel SG and Dutton JC. Velocity measurements of compressible turbulent mixing layers. *AIAA J* 1991; 29: 538–546.
5. Barre S, Quine C and Dussauge J. Compressiblity effects on the structure of supersonic mixing layers: experimental results. *J Fluid Mech* 1994; 259: 47–78.
6. Clemens NT and Mungal MG. Large-scale structure and entrainment in the supersonic turbulent mixing layer. *J Fluid Mech* 1995; 284: 171–216.
7. Tam CKW and Hu FQ. *Instabilities of supersonic mixing layers inside a rectangular channel*. AIAA Paper No. 88-3675-CP. Reston, VA: AIAA.
8. Greenough J, Riley J, Soetrisno M et al. *The effect of walls on a compressible mixing layer*. AIAA Paper No. 89-0372. Reston, VA: AIAA.
9. Zhuang M, Dimotakis PE and Kubota T. The effect of walls on a spatially growing supersonic shear layer. *Phys Fluids* 1990; A2: 599–604.
10. Morris PJ, Giridharan MG and Viswanathan K. *Turbulent mixing in plane and axisymmetric shear layers*. AIAA Paper No. 90-0708. Reston, VA: AIAA.
11. Lu PJ and Wu KC. Numerical investigation on the structure of a confined supersonic mixing layer. *Phys Fluids* 1991; A3: 3063–3069.
12. Liou TM, Lien WY and Hwang PW. Compressibility effects and mixing enhancement in turbulent free shear flows. *AIAA J* 1995; 33: 2332–2338.
13. Chakraborty D, Mukunda HS and Paul PJ. Two dimensional direct numerical simulation of nonreacting confined supersonic mixing layer. *Aeronaut J* 2000; June: 291–296.
14. Li Q and Fu S. Numerical simulation of high-speed planar mixing layer. *Comput Fluid* 2003; 32: 1357–1377.
15. Fiedler HE, Nayeri C, Spieweg R, et al. Three-dimensional mixing layers and their relatives. *Exper Thermal Fluid Sci* 1998; 16: 3–21.
16. Oh CK and Loth E. *A numerical investigation of supersonic turbulent shear layers: compressibility effects*. AIAA Paper No. 94-2244. Reston, VA: AIAA.
17. Erdos J, Tamagno J, Bakos R, et al. *Experiments on shear layer mixing at hypervelocity conditions*. AIAA Paper No. 92-0628. Reston, VA: AIAA.
18. Drummond JP. Supersonic reacting internal flow field, in numerical approaches in combustion modeling. In: ES Oran and JP Borris (eds) *Progress in aeronautics and astronautics*. AIAA, vol. 135: 1991, pp.365–420.
19. Carpenter MH and Kamath H. Three dimensional extension to the SPARK combustion code. NASA-CP-5029. Hampton, Virginia: NASA-Langley, 1988, pp.107–137.
20. Carpeter MH. *A generalized chemistry version of SPARK*. NASA-CR-4196. Hampton, Virginia: NASA, 1998.
21. Lian C, Merkle CL and Xia G. Flow field initialisation and approach to stationary conditions in unsteady combustion simulations. *Comput Fluids* 2010; 39: 310–323.
22. Clemens NT and Mungal MG. Two- and three-dimensional effects in the supersonic mixing layers. *AIAA J* 1992; 30: 973–981.
23. Sandham N and Reynolds W. *The compressible mixing layer: linear theory and direct simulation*. AIAA Paper No. 89-0371. Reston, VA: AIAA.
24. Wantuck PJ, Tennant RA, Rothstein AD, et al. *An experimental investigation of the properties of a non-reacting, supersonic shear layer*. AIAA paper 91-0628. Reston, VA: AIAA.
25. Risha DJ. *Analysis of growth rates in three-dimensional air-to-air, supersonic shear layers using direct numerical simulation*. AIAA Paper No. 95-0523. Reston, VA: AIAA.
26. Oh CK and Loth E. Effects of initial conditions on spatially evolving compressible shear layer simulations. *Comput Fluid Dyn* 1996; 6: 307–319.
27. Goebel SG and Dutton JC. *Velocity measurements of compressible, turbulent mixing layers*. AIAA Paper No. 90-0709. Reston, VA: AIAA.
28. Gruber MR, Messersmith NL and Dutton JC. *Three-dimensional velocity measurement in a turbulent compressible mixing layer*. AIAA Paper No. 92-3544. Reston, VA: AIAA.

Appendix

Notation

b	shear layer thickness
U	mean velocity in axial direction
$\bar{U}$	normalised mean axial velocity
U_1	inlet velocity of lower speed stream
U_2	inlet velocity of higher speed stream
y	lateral direction coordinate
y_o	location in lateral direction with the mean axial velocity as $(U_1 + U_2)/2$
η	similarity co-ordinate in lateral direction
σ_u	normal component of Reynolds stress in axial direction
σ_v	normal component of Reynolds stress in lateral axial direction
σ_w	normal component of Reynolds stress in span wise direction